Available online at www.sciencedirect.com
SCIENCE DIRECT®
ACADEMIC PRESS
Bioorganic Chemistry 30 (2002) 396–419
BIOORGANIC CHEMISTRY
www.elsevier.com/locate/bioorg

Solution structure and design of dithiophosphate backbone aptamers targeting transcription factor NF-κB ☆

David E. Volk,[a] Xianbin Yang,[a] Susan M. Fennewald,[b] David J. King,[a] Suzanne E. Bassett,[a] Sheela Venkitachalam,[a,1] Norbert Herzog,[b] Bruce A. Luxon,[a] and David G. Gorenstein[a,*]

[a] *Sealy Center for Structural Biology and Department of Human Biological Chemistry and Genetics, The University of Texas Medical Branch at Galveston, 301 University Boulevard, Galveston, TX 77555-1157, USA*

[b] *Department of Pathology and The WHO Collaborating Center for Tropical Diseases, The University of Texas Medical Branch, Galveston, TX 77555-1157, USA*

Received 13 July 2001

Abstract

A variety of monothio- and dithiosubstituted duplex aptamers targeting NF-κB have been synthesized and designed. The specificity and affinity of the dithioate aptamers of p50 and RelA(p65) NF-κB homodimers was determined by gel shift experiments. The NMR solution structures for several unmodified and dithioate backbone modified 14-base paired duplex aptamers have been determined by a hybrid, complete matrix (MORASS)/restrained molecular dynamics method. Structural

☆ This research was supported by DARPA (9624-107 FP), NIH (ES06676 and AI27744), and the Welch Foundation (H-1296) grants to D.G.G., N.H., and B.A.L. Building funds were provided by the NIH (1CO6CA59098). The project was funded in part by a NIH fellowship to D.E.V. (T32 AI07536).

* Corresponding author. Fax: +1-409-747-6850.
E-mail address: david@nmr.utmb.edu (D.G. Gorenstein).
[1] Present Address: Department of Bioengineering and Environmental Health, 56-786, Massachusetts Institute of Technology, Cambridge, MA 01239, USA.

0045-2068/02/$ - see front matter
doi:10.1016/S0045-2068(02)00510-2

perturbations of the dithioate substitutions support our hypothesis that the dithioate binds cations less tightly than phosphoryl groups. This increases the electrostatic repulsion across the B-form narrow minor groove and enlarges the minor groove, similar to that found in A-form duplexes. Structural analysis of modeled aptamer complexes with NF-κB homo- and heterodimers suggests that the dithioate backbone substitution can increase the aptamer's relative affinity to basic groups in proteins such as NF-κB by helping to "strip" the cations from the aptamer backbone.

Keywords: NF-κB; Dithioates; Monothioates; Antisense; NMR; Solution structure

1. Introduction

The NF-κB/Rel transcription factor family mediates inducible transcriptional activity of multiple immune and acute phase response genes in a variety of cell types [1–4]. Members of this protein family can be divided into two groups based on differences in their structures, functions and modes of synthesis: one group consists of the precursor proteins p105 and p100 with ankyrin repeat domains in their carboxy termini. Proteolytic processing removes their carboxyl halves to yield the mature forms p50 and p52, respectively, whose homodimers are weak transcriptional activators because they lack the transactivation domains. A second group, including RelA(p65) (RelA), c-Rel, v-Rel, Rel B, Dorsal, and Dif are not synthesized as precursors and are sequestered in the cytoplasm by association with inhibitors (IκB) or precursor proteins (p100 and p105). Homo- or heterodimers consisting of at least one member from this group are strong transcriptional activators.

NF-κB is modulated by many factors that increase the inflammatory response. Their activation leads to the coordinated expression of many genes that amplify and perpetuate the immune response [5] and pathogenic responses, including toxic shock. NF-κB is, therefore, an obvious target for new types of anti-inflammatory treatments. Current anti-inflammatory treatments such as glucocorticoids [6], anti-oxidants [7], and naturally occurring NF-κB inhibitors such as gliotoxin [8] all have concerns regarding selectivity, effectiveness, toxicity, or side-effects. More importantly, given the data for single and double knock out mice [9–11], prolonged inactivation of all NF-κB protein activities is likely inappropriate.

Another drug-targeting approach that has been pursued is the use of antisense oligonucleotides (AS-ODNs) [12]. Base pairing of the AS-ODN to target mRNA blocks the expression of the gene product by targeting the mRNA for RNase H mediated degradation, steric hindrance of translation, as well as inhibition of mRNA processing and transport. Preliminary results using AS-ODNs targeting RelA(p65)

Abbreviations used: rMD, restrained molecular dynamics; MORASS, multiple Overhauser relaxation analysis and simulation; EMSA, electrophoretic mobility shift assay; AS-ODN, antisense oligonucleotide; S-ODN, Monothiophosphate oligonucleotide; S_2-ODN, dithiophosphate oligonucleotide; GST, glutathione-*S*-transferase.

demonstrate the significant potential of these agents in inhibiting inflammatory bowel disease mimicking human Crohn's disease [13].

Unfortunately, inhibiting the synthesis or the elimination of any one member of the NF-κB family will eliminate all the possible dimers of which that protein would be a normal subunit. Thereby, AS-ODNs and knock out mice make it impossible to determine the precise roles of specific NF-κB dimers in regulating gene expression and their associated physiological and pathophysiological processes. Furthermore, broad inhibition of NF-κB may be unwise because these factors play such a critical part in the immune response and other defensive responses. Therefore, the development of specific inhibitors of individual NF-κB dimers would permit the identification (and modulation) of specific regulatory sets of genes for individual NF-κB homo- and heterodimers.

An alternative ODN approach that provides this increased specificity involves the use of aptamer or decoy ODNs by which double stranded DNA sequences representing binding sites for specific transcription factors can be used to compete for protein binding to the authentic binding elements in cellular DNA [14]. Sharma et al. [15] used a decoy ODN, termed CK-1, representing the NF-κB binding site in the G-CSF and GM-CSF promoter to which RelA, but not the p50 homodimer, which binds to inhibit tumor cell growth in vitro and in vivo (see below) [16]. They used the CK-1 decoy ODN to decrease the expression of cytokine and immunoglobulin genes in cultured mouse splenocytes. It was argued that CK-1 specifically targeted the activators of NF-κB regulated gene expression, p50/c-Rel or RelA dimers, and not the repressive p50 homodimers. Decoy ODNs were used in vivo to improve rat heart tolerance against ischemia-reperfusion injury in association with the inhibition of neutrophil adherence and tissue IL-8 production [17]. Decoy ODNs targeting NF-κB have also been used to demonstrate the role of NF-κB in regulating cyclooxygenase expression following hypoxia [18] and regulation of apoptosis in B chronic lymphocytic leukemia cells [19].

Recently, decoy ODNs were developed to inhibit expression from CRE and AP-1-directed transcription in vivo and inhibit growth of cancer cells in vitro and in vivo [20]. These studies and others [15,21–27] demonstrated the potential of the approach of using specific decoy ODNs to dissect the role of transcription factors and particularly NF-κB dimers in regulating the expression of various genes. Decoy ODNs represent far more specific agents to be used in the modulation of pathogenic immune responses (such as septic shock) or the expression of adhesion molecules involved in chronic immune disorders and cancer.

It is unlikely, however, that the phosphodiester form of ODNs is appropriate for cell culture or therapeutic use because of its short half-life in cells and serum due to DNase digestion [28]. Backbone modifications such as phosphorothioate (S-ODN) and phosphorodithioate (S_2-ODN) internucleoside linkages which decrease the nuclease hydrolysis of the aptamers are therefore needed. To this end, we have synthesized and designed a variety of monothio- and dithiosubstituted duplex aptamers targeting NF-κB and studied both their specificity and affinity as well as NMR solution structures and modeled complex with NF-κB. Structural perturbations of the dithioate substitutions support our hypothesis that the dithioate binds cations less tightly than phosphoryl groups. The structural analysis suggests that the dithioate

backbone substitution can increase the aptamer's relative affinity to basic groups in proteins such as NF-κB by helping to "strip" the cations from the aptamer backbone.

2. Materials and methods

Preparation and purification of the oligonucleotides. Oligonucleotides with normal phosphodiester backbones were synthesized on a 1.3-μmol scale using standard phosphoramidite chemistry on a Gene Assembler Plus DNA Synthesizer. Oligonucleotides containing phosphorodithioates were synthesized on either a 1 or 15 μmol scale using phosphorothioamidite chemistry [29] on an Expedite 8909 DNA Synthesizer as previously described [30]. The thiophosphite triesters were oxidized with the sulfurization reagent EDITH [31]. After removal of the dimethoxytrityl group the crude oligonucleotides were purified on a Mono Q HR 10/10 FPLC column (Pharmacia) with a flow rate of 2.0 ml/min using a linear gradient of two buffers. Buffer A contained 25 mM Tris–HCl and 1 M EDTA at pH 8, and buffer B contained 25 mM Tris–HCl, 1 mM EDTA and 1.0 M NaCl at pH 8. Buffer B was increased linearly from 0–100% over an 80-min interval. Retention times were approximately 10–30 min shorter for the normal backbone oligonucleotides relative to the dithioated oligonucleotides. The purified oligonucleotides were desalted and concentrated by ultra-filtration using Centricon-3 (Amicon) centrifugal concentrators. Equal molar quantities of complementary strands were mixed, annealed at 90 °C, and slowly cooled to form the duplexes CK14, XBY2, and XBY6.

Protein expression and purification. Human NF-κB proteins p50 and RelA(p65) were expressed in *Escherichia coli* BL21 cells using the pGEX vector (AP Biotech), an IPTG inducible system that allows cloning and efficient purification of glutathione S-transferase fusion proteins. Typically, a 20-liter culture of RelA(p65) or p50 was processed as follows. The bacteria were grown in LB media at 37 °C to an OD_{600} of 0.5 and induced for 4 h by the addition of IPTG to a final concentration of 1 mM. The cells were harvested by centrifugation (5 min at 5000*g*) and resuspended in high salt buffer containing 1 mM EDTA, 1 M NaCl, and 20 mM NaH_2PO_4 at pH 7. To inhibit protease activity, 1 μg/ml aprotinin and 1 μM PMSF were added. A low salt buffer containing 1 mM EDTA, 150 mM NaCl and 20 mM NaH_2PO_4 at pH 7 was used in all subsequence chromatographic separations. Lysozyme (1 mg/ml final concentration) was added to the resuspended cells which were subsequently subjected to three freeze/thaw cycles with sonication. The lysate was centrifuged (10,000*g*) and the soluble fraction was loaded onto a glutathione Sepharose affinity column (25 mm/45 cm) preequilibrated with high salt buffer. The column was washed with high salt buffer to remove bacterial nucleic acids and proteins until a baseline UV spectrum was achieved at all wavelengths and subsequently was washed with low salt buffer in preparation for thrombin cleavage. Thrombin (1000 U) was then loaded onto the affinity column and allowed to incubate overnight at 4 °C. The cleaved protein was eluded with low salt buffer, concentrated to 10 ml, and passed through a Mono Q column (25 mm/200 cm). Fractions containing RelA(p65) (or p50) were pooled and passed through a Q sepharose column (25 mm/50 cm) producing soluble, active protein that was greater than 99% pure as measured by 4–20% gradient SDS–PAGE.

^{32}P labeling of oligonucleotides. Unmodified DNA (HPLC-purified) was purchased (Biosynthesis, Lewisville, TX) and each strand was stored in aliquots at 100 μM at −20 °C prior to labeling. The DNA was ^{32}P labeled using T4 polynucleotide kinase and [γ-^{32}P]dATP, and the unincorporated nucleotide was removed by gel filtration in water. The labeled DNA strands were lyophilized and subsequently resuspended in binding buffer prior to quantification. Equal amounts of complementary DNA were combined and annealed, and the purity of each duplex was assessed on an 8% polyacrylamide TBE gel.

Nuclear extract preparation. Nuclear extracts were prepared following standard procedures. Pelleted cells were resuspended in buffer I with sucrose (0.32 M sucrose, 3 mM of $CaCl_2$, 2 mM MgAcetate, 0.1 mM EDTA, 10 mM Tris, pH 8.0, 0.5 mM PMSF). Nuclei were pelleted, washed in buffer I without sucrose and repelleted. Nuclei were then resuspended in a low salt buffer (20 mM Hepes, pH 7.9, 25% glycerol, 1.5 mM $MgCl_2$, 20 mM KCl, 0.2 mM EDTA, 0.5 mM PMSF), an equal volume of high salt buffer (20 mM Hepes pH 7.9, 25% glycerol, 1.5 mM $MgCl_2$, 0.8 M KCl, 0.2 mM EDTA, 0.5 mM PMSF) was added, and the nuclei were incubated on ice for 20 min. They were then diluted by the addition of 2.5× vol of dilution buffer (25 mM Hepes, pH 7.6, 25% glycerol, 0.1 mM EDTA, 0.5 mM PMSF) and debris was pelleted. The supernatant was removed as nuclear lysate and stored at −80 °C.

Electrophoretic mobility shift assays (EMSAs): Method 1. For EMSA reactions, 1–5 μg of nuclear extract or 10–50 ng of purified recombinant NFκB RelA(p65) or p50 was incubated with 0.1 pmol of radiolabeled oligonucleotide in a 15-μl vol under standard reaction conditions (20 mM Hepes, pH 7.5, 50 mM KCl, 2.5 mM $MgCl_2$, 20 mM DTT, 50 μg/ml polydIC, 10% glycerol, 0.1 mg/ml BSA). Oligonucleotides were end labeled with [γ-^{32}P]ATP using T4 polynucleotide kinase (New England Biolabs, Beverly, MA). For competition experiments, cold oligonucleotide (0.001–10 μM) was also added at the start of the reaction. After 15 min, the reaction was loaded onto a standard 6% polyacrylamide gel in 0.25× TBE (22 mM Tris-Base, 22 mM boric acid, 0.5 mM EDTA). Following electrophoresis, the gel was dried and quantified using a Packard InstantImager. Images for figures were derived from exposure to XAR-5 film.

Electrophoretic mobility shift assays (EMSAs): Method 2. The binding affinities of the NF-κB proteins were analyzed using electrophoretic mobility shift assays (EMSA) run on native 8% polyacrylamide gels which contained 22 mM Tris-base, 22 mM boric acid, 0.5 mM EDTA, 8% acrylamide, 0.075% bisacrylamide, 2.5% glycerol, 0.0675% APS, and 0.075% Temed. The gels were cooled to 4 °C before the binding reactions were loaded. The buffer conditions of the binding reactions were 10 mM KH_2PO_4, 100 mM NaCl, 0.1 mM EDTA, 5 mM $MgCl_2$, 40 mM DTT, 6% glycerol, and 1 mg/ml BSA at pH 7. For each isotherm the RelA(p65) (or p50) and inhibitor DNA concentrations were fixed and IgκB was titrated in. After a 1-h incubation period, tracking dye was added and the 50-μl reactions were loaded onto the gels. The gels were run for 60 min at 1 milliamp/cm^2 until the xylene cyanol and bromophenol blue bands were resolved. After drying, the radioactivity (in cpm) of the gel bands was measured on a Packard Instant Imager. A more thorough description of these experiments and the dissociation constants derived from them will be published elsewhere [63].

NMR spectroscopy. All proton experiments were carried out on Varian UNITYplus 750 or 600 spectrometers. NOESY experiments were carried out using the WET-NOESY pulse sequence [32]. NOESY experiments carried out in 99.96% D_2O were done at 15 °C at 750.258 MHz with 4096 complex points t_2 and 512 complex points in t_1, sweep widths of 7455.7 Hz and a relaxation delay of 4.3 s. The 200 ms mixing time NOESY carried out in 90% H_2O/10% D_2O was done at 5 °C at 599.800 MHz with 8192 complex points in t_2 and 512 complex points in t_1, sweep widths of 12,001 Hz, and a relaxation delay of 3.8 s. Ninety degree shifted sine-bells were applied to both dimensions of the NOESY experiments before Fourier transformation. Z-filtered TOCSY [33] experiments were recorded with 50 and 120 ms mixing times. DQF-COSY [34] experiments were recorded at 15 °C. The data were processed using VNMR on SUN Sparc 10 and Sparc 20 workstations or Silicon Graphics (SGI) workstations.

Restrained molecular dynamics calculations. The NMR structure refinements followed a MORASS/AMBER protocol that has been previously described [35]. Calculations were performed on a SGI Indigo2 workstation. Nonexchangeable proton distance constraints were derived from our hybrid relaxation matrix program, MORASS 2.5 [36], using NOE volumes from 200 ms NOESY spectra done in 99.96% D_2O. A total of 601, 459, and 483 flat well constraints (including 14 imino proton constraints) were used for refinement of CK14, XBY2 and XBY6, respectively, during our 5 ps AMBER 5 [37] molecular dynamics simulations at 300 K. The coordinates of the last 1 ps of MD were averaged using CARNAL [38] and this average coordinate set was refined by 2000 steps of full conjugate gradient minimization without NOESY restraints. The starting structures for these calculations were standard B form DNA that contained phosphorodithioate substitutions where appropriate. Amber force field bond length and angle parameters for the dithioated bases were determined from ab initio calculations at the 6–31G* level and point charges were determined using the RESP program [39].

The progress of the iterative refinement process was monitored by several key factors, indicating the match between experimental NOESY volumes and theoretical NOESY volumes calculated from the refined structure. The rms errors in the volumes were used as the first criterion for monitoring the refinements [40]. The %rms (volume) is given by

$$\%\text{rms (volume)} = \sqrt{1/N \sum_{ij} \left(\frac{v_{ij}^a - v_{ij}^b}{v_{ij}^a} \right)^2} \times 100\%,$$

where a or b can be either the experimental or theoretical 2-D vol to give the %rms (exp) or %rms (the), respectively.

The R factor that is similar to the R factor used in X-ray crystallography was also used as a refinement criteria. The R factor is given by,

$$R = \frac{\sum_{ij} \left| v_{ij}^a - v_{ij}^b \right|}{\sum_{ij} v_{ij}^a},$$

where a represents experimental volumes and b represents theoretical volumes.

We have suggested that the %rms (volume) is a very useful measure of quality of fit to the spectra since it weighs the percentage differences in the theoretical and

experimental volumes for both large and small cross peaks equally. The R factor is regarded as a poorer measure of the quality of the refined structure since it is often dominated by the largest cross peaks. Another quality of fit, the $Q^{1/6}$ factor [41], also better reflects the quality of the structure since it weighs more heavily on the weak cross peaks (longer, inter-residue distances) compared to the R factor. The $Q^{1/6}$ factor is defined as,

$$Q(1/6) = \frac{\sum_{ij} \tau_m \left| (v_{ij}^a)^{1/6} - (v_{ij}^b)^{1/6} \right|}{\sum_{ij} (1/2) \tau_m \left| (v_{ij}^a)^{1/6} + (v_{ij}^b)^{1/6} \right|},$$

where a represents theoretical volumes and b represents experimental volumes.

A 70-ps unrestrained molecular dynamics calculation was undertaken using the final structures from the last round of the MORASS/rMD/minimization cycles for each duplex as the starting structures, and the 50 lowest energy structures from the last 50 ps were minimized. The 50 structures were grouped into clusters using the CalcCluster module in MolMol [42] with a maximum RMSD of 1 Å within each cluster. An average structure was determined for the 10 clusters containing the greatest number of structures (CARNAL [38]) and these averaged structures were refined by 2000 steps of unconstrained full conjugate gradient minimization to yield 10 starting structures for each duplex. For each duplex, the 10 structures were subjected to 5 ps of rMD followed by unconstrained minimization. The coordinates of these ten final structures were then averaged (CARNAL) and subsequently minimized without restraints to provide the final average structure for each duplex. All structures were built with XLEAP [43] and displayed with MolMol or MIDAS2.1 [44].

3. Results

Sharraa et al. [15] have previously demonstrated effective aptamer inhibition of NF-κB activity. They further achieved NF-κB activity inhibition in cell culture using monothiophosphate duplex decoys of the NF-κB binding consensus-like sequence d(GGGGACTTCC). Our initial approach used the "CK-1" 42-mer duplex oligonucleotide identified by Sharma et al. (Note: both ours and Sharma et al.'s [S]-ODN duplex was chemically synthesized by sulfur oxidation with phosphoramidite chemistry and thus contains in principle 2^{82} or 10^{24} different stereoisomers). The wild-type CK-1 duplex sequence comprises 3 tandem repeats of a 14 mer NF-κB consensus-like sequence d(5′-CCA GGA GAT TCC ACC CAG GAG ATT CCA CCC AGG AGA TTC CAC 3′). Our studies, using recombinant protein homodimers of p50, RelA(p65), and c-Rel, confirmed the published results showing that the CK-1 sequence could bind to and compete for binding to RelA(p65) homodimer but not p50 homodimer in standard electrophoretic mobility shift assays (EMSA, Method 1) (Fig. 1). In addition, we found CK-1 also bound to and competed for binding to c-Rel (data not shown). Oligonucleotides containing only one copy of the binding site, in either a 14-mer (5′-CCA GGA GAT TCC AC; CK14) or a 22-mer duplex ODN (an IgκB site), behaved similarly to the longer CK-1 version (data not

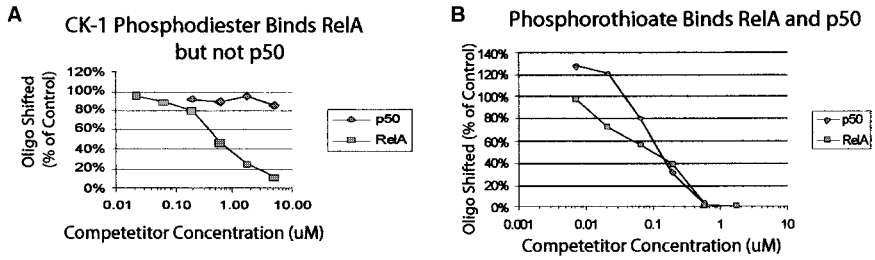

Fig. 1. Competitive electrophoretic mobility shift assays (EMSA), using recombinant protein homodimers of p50 or RelA(p65), with the CK1 42-mers, having either normal backbone (A) or monothiophosphate backbone (B).

shown), and they served as our first target for the synthesis of various hybrid backbone-modified aptamers.

While the phosphodiester form of CK-1 bound RelA(p65)/RelA(p65) and not p50 homodimer, [Fig. 1A], the fully substituted phosphorothioate CK-1 aptamer [Fig. 1B] inhibited both RelA(p65)/RelA(p65) and p50/p50 equally. Varying the reaction conditions did not produce sequence-specific inhibition for the [S]-ODN nor the NF-κB protein dimer specific inhibition originally observed with the phosphodiester versions of the CK-1 decoy oligonucleotides. This suggests that [S]-ODNs with large numbers of phosphorothioate linkages are "sticky" and tend to bind "nonspecifically" to proteins. It is assumed that the sulfur substitutions are responsible for this loss in dimer specificity. We have found that if the number of phosphorothioate linkages is reduced to only 2–4, the specificity can be restored, but binding is not enhanced.

When we attempted to demonstrate the inhibition of binding studies using cell extracts containing native NFκB dimers, we encountered additional and unexpected difficulties. The CK-1 aptamer, in the wild-type diester form, does not compete effectively for NF-κB binding in nuclear extracts of the 70Z/3 pre B cell line or the RAW 264.7 mouse macrophage-like line (data not shown). It is possible that the heterodimers present in these cells either do not bind the CK-1 sequence tightly enough or that the CK-1 aptamer is bound by other cellular components.

The fully thioated aptamers are also problematic in cell extracts. When fully monothioated, the sequences CK-1, mutant CK-1, IgκB, and mutant IgκB all inhibit NF-κB binding in vitro, but fail to bind specifically to NF-κB generating smears the length of the EMSA gel lane indicating nonspecific binding of these thioated oligonucleotides to numerous cellular proteins (data not shown). Therefore, even with sequences with good binding and specificity in the diester form, when fully thiophosphate substituted, they lose their sequence specificity. Thus, this sticky nature of fully thioated aptamers makes their characterization in vitro not necessarily predictive of their activities in vivo (see [30]).

CK14 dithioate aptamers. The CK14 14-mer duplexes with some strategically placed dithioate internucleoside linkages have been synthesized to determine the influence of sulfur substitutions on affinity (Tables 1 and 2). While binding affinity is enhanced and specificity is altered depending upon the number and site of dithioate

Table 1
DNA duplexes synthesized

IGκB	5′-GCCTGGGAAAGTCCCCTCAACT-3′ 3′-CGGACCCTTTCAGGGGAGTTGA-5′		
CK1	5′-CCAGGAGATTCCACCCAGGAGATTCCACCCAGGAGATTCCAC-3′ 3′-GGTCCTCTAAGGTGGGTCCTCTAAGGTGGGTCCTCTAAGGTG-5′		
CK14	5′-CCAGGAGATTCCAC-3′ 3′-GGTCCTCTAAGGTG-5′	XBY13	5′-CCAGGAGATT**CC**AC-3′ 3′-GGT**CC**T**C**TAAGGTG-5′
XBY1	5′-CCAGGAGATTCCAC-3′ 3′-GG**T**CCTCTAAGG**T**G-5′	XBY14	5′-C**C**AGGAGATT**CC**AC-3′ 3′-GGTCCTCT**AA**GGTG-5′
XBY2	5′-CCAGGAGATTCCAC-3′ 3′-GGTCC**T**C**T**AAGGTG-5′	XBY15	5′-CC**AG**GAGA**TT**CCAC-3′ 3′-GGT**CC**T**C**TAAGGTG-5′
XBY3	5′-CCAGGAGATTCCAC-3′ 3′-GG**T**CC**T**C**T**AAGG**T**G-5′	XBY16	5′-CCAGGAGA**TT**CCAC-3′ 3′-GGT**CC**T**C**TAAGGTG-5′
XBY4	5′-CCAGGAGA**TT**CCAC-3′ 3′-GGTCC**T**C**T**AAGGTG-5′	XBY17	5′-CCAGG**A**G**A**TTCC**A**C-3′ 3′-GGT**CC**T**C**TAAGGTG-5′
XBY5	5′-CCAGGAGA**TT**CCAC-3′ 3′-GG**T**CCTC**T**AAGG**T**G-5′	XBY18	5′-C**C**AGGAGATT**CC**AC-3′ 3′-GG**T**CCTCTAAGG**T**G-5′
XBY6	5′-CCAGGAGA**TT**CCAC-3′ 3′-GG**T**CC**T**C**T**AAGG**T**G-5′		

Note. Bases shown in bold contain a dithioated phosphate linkage on the 3′ side.

substitutions, they lack the extreme "stickiness" of the fully monothioated CK1 aptamer. When only one or two dithioate linkages are placed in the molecule, the inhibition/binding of the oligonucleotide to recombinant protein is similar to that of the unsubstituted oligonucleotide. As more substitutions are made the binding by the oligonucleotide increases dramatically (see Fig. 2 in [30]). One of the tightest binding dithioate aptamers, XBY6, contains 6 dithioate linkages on the two strands.

EMSAs (Method 2) were used to quantitatively determine the binding constants of IgκB and XBY6 towards RelA(p65) homodimers. For each binding isotherm, inhibitor DNA, either unlabeled IgκB or XBY6, was added to a fixed amount of RelA(p65) protein, and increasing amounts of radio-labeled IgκB were added into otherwise identical reactions. The K_d of IgκB (4 nM) was determined by using unlabeled IgκB as the inhibitor at various protein concentrations and by fitting the resulting data to a simple model with a 1:1 binding stoichiometry of RelA(p65) homodimers to IgκB. A second set of experiments was conducted (Fig. 2) using XBY6 as the inhibitor. At a given concentration of total IgκB, the ratio of bound IgκB/RelA(p65) homodimer decreases with increasing amounts of XBY6 in the reactions. Using the 4 nM K_d of IgκB, the entire data set was globally fit to determine that the thioaptamer XBY6 binds with K_d of 1.44 nM to the RelA(p65) homodimer [63].

Significantly, the XBY6 aptamer is also able to bind to a single NF-κB complex present in nuclear extracts (see Fig. 3 in [30]), while the CK-1 and CK14 oligonucleotides show no NF-κB specific binding in cell nuclear extracts. This shows that a

Table 2
Analysis of the MORASS/MD generated structures of CK14, XBY2, and XBY6

NMR distance constraints	CK14	XBY2	XBY6
Total NOE distance restraints	601	459	483
Interresidue restraints	229	155	166
Intraresidue restraints	372	304	317
H-bonding restraints (empirical)	14	14	14
Structural Statistics			
NMR $Q^{1/6}$ factor			
Final averaged structure	0.0742	0.0780	0.0775
Best fitting structure	0.0726	0.0741	0.0733
Worst fitting structure	0.0815	0.0792	0.0786
rmsd of NOE violations (Å)			
NOE violations >0.5 Å	40 ± 7	43 ± 4	19 ± 3
NOE violations >0.3 Å	113 ± 6	93 ± 4	51 ± 5
RMS deviations from ideal geometry			
Bond length (Å)	0.029 ± 0.001	0.029 ± 0.001	0.029 ± 0.001
Bond angle (°)	4.04 ± 0.05	4.18 ± 0.06	4.11 ± 0.08
Pairwise rmsd (Å) over heavy atoms of central 12 bp			
Final ave versus starting model	1.91	2.36	2.85
Final ave versus 10 tructures	0.72 ± 0.27	0.83 ± 0.12	0.92 ± 0.16

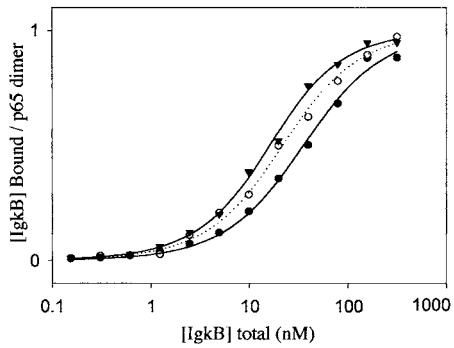

Fig. 2. EMSA of IgκB DNA:RelA(p65)$_2$ in the presence of inhibitor XBY6. Three fixed amounts of XBY6 concentrations were used (1.95 (▼), 3.89 (○), and 7.77 (●) nM).

thioate backbone modification can increase both the affinity and specificity of the oligonucleotide to NF-κB above that of other cellular proteins. This demonstrates the feasibility of altering specific-binding ability by the substitution of a limited number of internucleoside linkages. It also appears to have provided an aptamer that is able to distinguish among various NF-κB dimers within the cell.

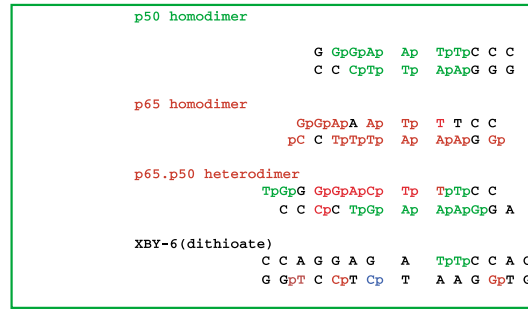

Fig. 3. NF-κB contacts to DNA. For p50 and RelA(p65) homo- and heterodimers, phosphate contacts between the p50 subunit-are shown in green, while phosphate contacts to the RelA(p65) subunit are shown in red (based upon cystral structures, [45–48]). Proposed contacts of the dithiophosphates of XBY6 are shown in green and red.

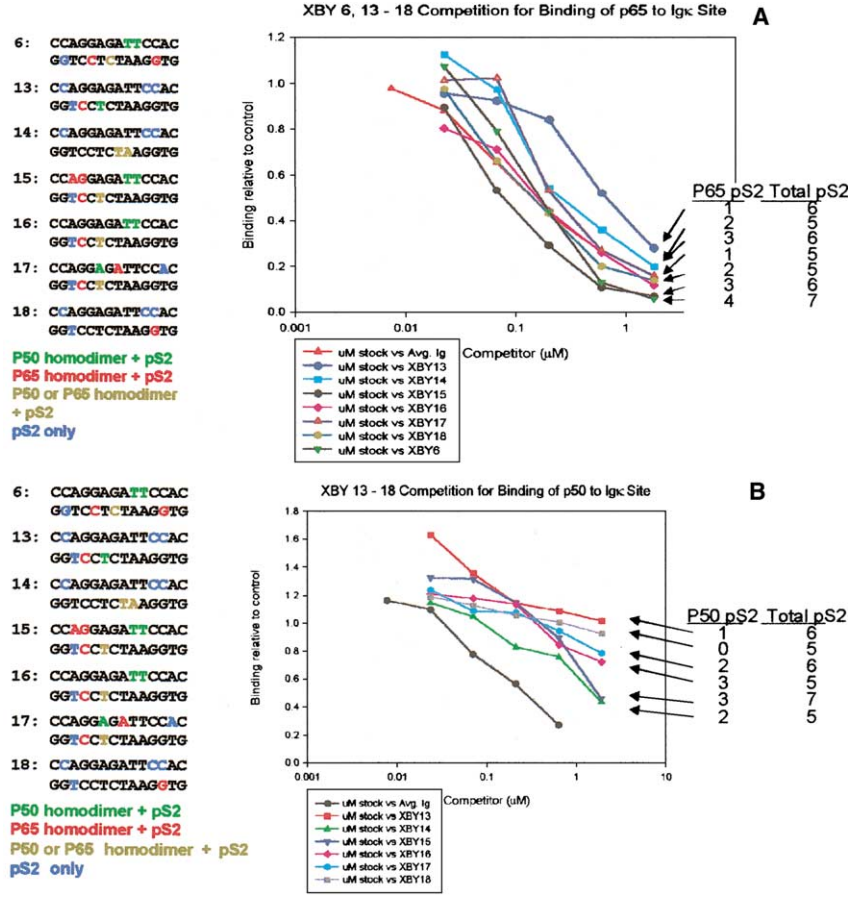

Fig. 4. Competive EMSA binding curves for various dithioated aptamers with RelA(p65) (A) and p50 (B). The sequence is that of CK14 with dithioated substitutions (see Table 1).

Structural basis for dithioate aptamer binding specificity. To better understand the enhanced binding of the dithioated CK14 analogs, we have studied the solution structures of the CK14, XBY2 and XBY6 duplexes and modeled their interactions with the NF-κB dimers.

Using AMBER5, MIDAS, and MOLMOL, the XBY6 thioaptamer was modeled into the 1vkx PDB coordinate file of a p50/RelA(p65) NF-κB heterodimer DNA cocrystal structure [45] and the protein-DNA close contacts were calculated. All but one of the six dithio-substituted nucleotides in the NF-κB·XBY6 model structure make close H-bond contacts to the protein side chains of the heterodimer (R15, R17, C20, E21, E295, K379, K380, K476) similar to those of the unsubstituted cocrystal DNA. The single dithioate that makes no apparent protein contacts is the penultimate base on the second strand of the aptamer.

Based upon the hypothesis that enhanced affinity of the dithioate aptamers for the NF-κB dimers will correlate with proximity of the modified phosphate to a protein binding site (largely a basic amino acid side chain), we have predicted that the greater the number of such interactions, the greater the affinity. As shown in Fig. 3, based upon the crystal structures of duplex sites bound to various NF-κB dimers [45–48], a number of phosphates (shown in color) are in close contact with groups on the NF-κB dimers. The p50 homodimer phosphate contacts (colored) are localized to the center of the duplex. (Interestingly, although the duplexes in the p50 and RelA(p65) homodimers have palindromic symmetry, the dimer contacts are asymmetric.) In both the heterodimer and the RelA(p65) homodimer, contacts are extended further from the center of the duplexes. In addition, phosphate contacts are not observed in the 5′TTCC3′ half site for the RelA(p65) homodimer, whereas these contacts are observed for the p50 homodimer and in the p50 subunit in the p50/RelA(p65) heterodimer. (Analysis of the contacts is complicated by the different sequence contexts and proper registration of the DNA—indeed for the RelA(p65) homodimer, a better argument based upon the identity of the amino acid side chains contacting the phosphates could be made to shift the sequence 1 nt to the right).

It is very intriguing that our XBY-6 dithioate substituted CK14 (6 dithioate substitutions indicated in colored phosphates) has the highest specificity and strongest affinity of any of the monothioate, unmodified, or dithioate CK14 aptamers for a specific p50-containing heterodimer. Note that the dithioate positions favor a p50 interaction ($\underline{TpS_2TpS_2}$C C) as well as a RelA(p65) interaction, by having dithiophosphates further removed from the center of the site.

Additional dithiophosphate modified CK14 aptamers were next synthesized to take advantage of the putative differential effects for dithioate interactions and stabilization of the complexes. Shown in Fig. 4 are the competitive binding EMSA plots for binding of these additional 14-mer duplexes with varying positions and numbers of dithioate substitutions. In general the results follow the prediction that affinity is highest for those dithioate aptamers containing the greatest number of favorable phosphate contacts to the specific dimer, as based upon our modeling.

Proton NMR spectra and chemical shift assignments. The DNA proton chemical shift assignments (see) were made utilizing NOESY, TOCSY, and DQF-COSY experiments and by following established methods for canonical DNA [49].

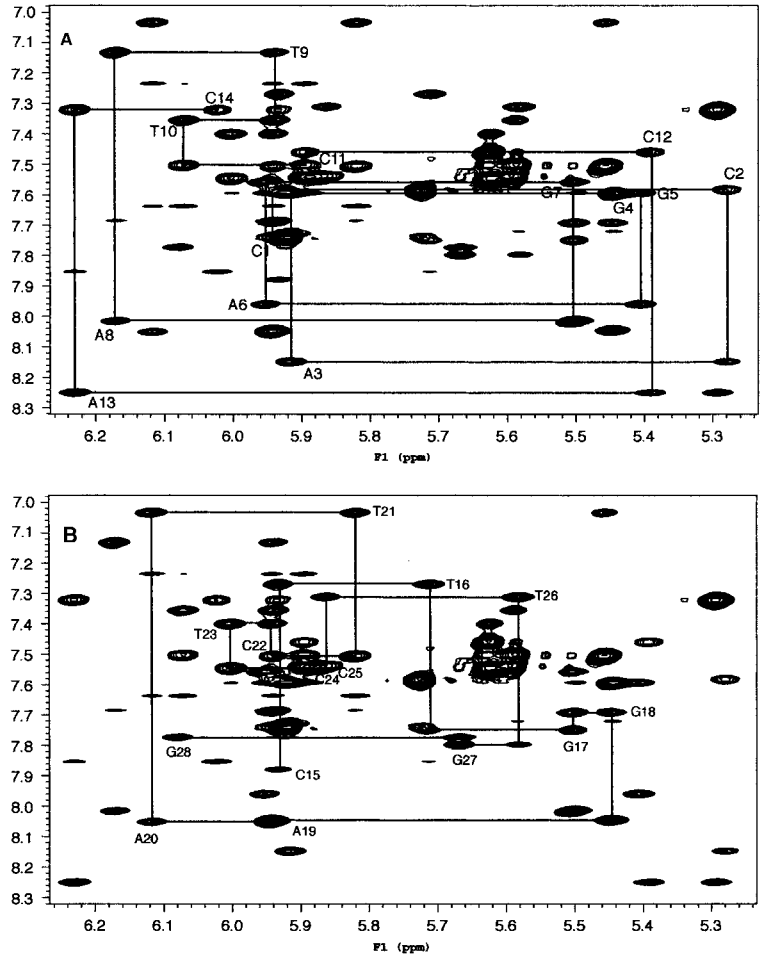

Fig. 5. The base to H1′ region of a 200 ms NOESY spectrum of CK14 in D_2O. Sequential connectivity is illustrated in A for one strand and in B for the complementary strand.

Fig. 5 shows the base to H1′ region of the 200 mixing time 2D NOESY spectrum taken for CK14. The sequential connectivity for one strand of the CK14 duplex, 5′-d(CCAGGAGATTCCAC)-3′ is shown by solid lines in Fig. 5A, and the connectivity for its complementary strand, 5′-d(GTGGAATCTCCTGG)-3′, is shown in Fig. 5B. Similar spectra are shown for XBY6 in Fig. 6.

Spectra were taken at both 15 and 25 °C to facilitate the assignments for the severely overlapped chemical shifts. Although the TOCSY spectrum of CK14 was severely overlapped in several regions, particularly the region around 5.94 ± 0.02 ppm, 26 of the 28 ring systems could be unambiguously assigned with the TOCSY data alone. The remaining two ring systems were assigned by considering the additional NOESY and DQF-COSY spectra. The proton chemical shifts of the two dithioated analogs, XBY2 and XBY6, are very similar to those of CK14,

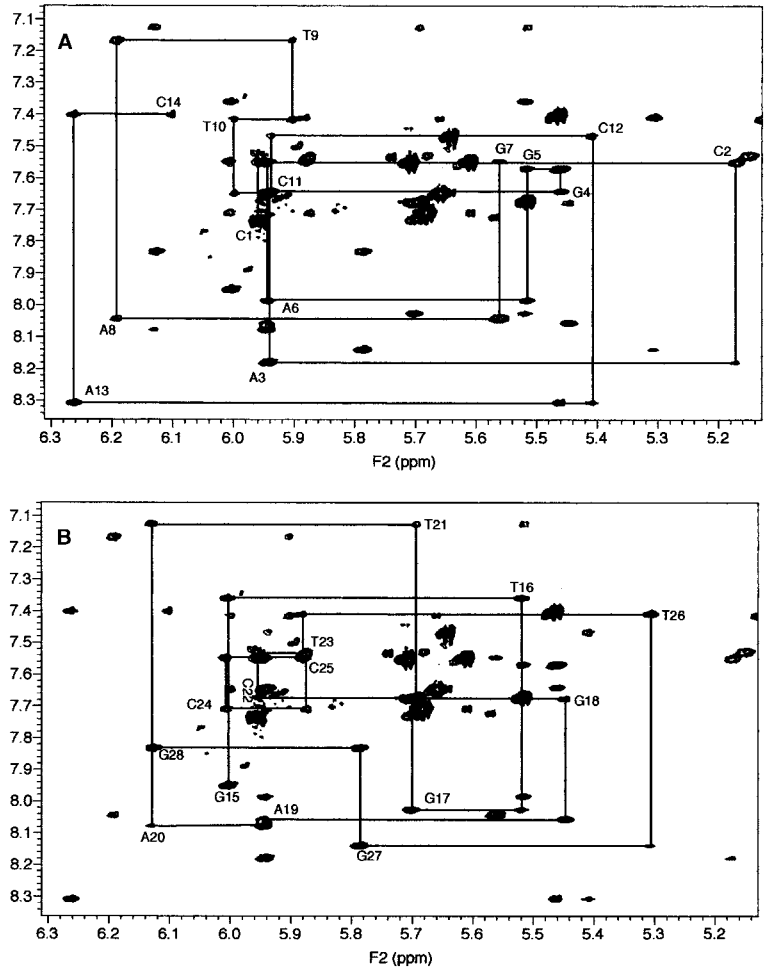

Fig. 6. The base to H1′ region of a 200 ms NOESY spectrum of XBY6 in D_2O. Sequential connectivity is illustrated in A for one strand and in B for the complementary strand.

although significant shifts (>0.1 ppm) were observed for protons near the dithioated residues (see supplementary material).

Structure refinements. For each of the duplexes, an iterative MORASS/rMD protocol [35] was followed and after 4 or 5 rounds all of the NOE volumes had merged (Tables S4–S6, supplementary material) and the total constraint energies were 283.4, 316.6, and 138.0 kcal/mol for CK14, XBY2, and XBY6, respectively. In the final round of MORASS of each duplex, each of the structural figures of merit, %rms(vol), $Q^{1/6}$ factor, and R factor indicated a good final fit to the NMR data. CK14, XBY2, and XBY6, respectively, yielded the following figures of merit: %rms(vol) = 76.4, 73.2, and 84.7; R factor = 0.4040, 0.3749, and 0.3855; $Q^{1/6}$ factor = 0.078, 0.074, and 0.072. Because NOE volumes are related to the interatomic

distance (r) by a $1/r^6$ factor, a %rms(vol) value of 84.7, as observed for XBY6, indicates less than an 11% error in the MORASS-derived distances versus the final model distances. The final structure obtained from the MORASS/rMD cycles for each of the duplexes was subjected to 70 ps of free MD and the 50 lowest potential energy structures in the last 50 ps were clustered to generate 10 starting structures for each of the duplexes (see experimental details). Each of the 10 starting structures were then subjected to 5 ps of rMD using the constraints obtained from the final MORASS cycle of each duplex and the coordinates of the last 1 ps were then averaged for each structure. The 10 structures thus obtained were subjected to 2000 steps of conjugate gradient energy minimization without constraints to obtain the 10 final structures for each duplex. Finally, these 10 structures were averaged to obtain the final average structure of each duplex. For CK14, XBY2, and XBY6, the RMSD of the heavy atoms of the central 12 bp for the 10 structures versus the final average structures were 0.72 ± 0.27, 0.83 ± 0.12, and 0.92 ± 0.16 Å, respectively. The averaged structures for CK14, XBY2, and XBY6 are shown in Fig. 7.

NOE violations. Considerably more constraint violations over 0.5 Å were observed in the CK14 structure refinement (40 ± 7) relative to the refinement of XBY6 (19 ± 3). This is due to the fact that 117 more NOEs were used in the CK14 refinement. Because this sequence is nonpalindromic. it has 28 unique residues, and the NOE spectra of these duplexes are very crowded. For the CK14 structure roughly one half of the constraints result from NOE volumes which are well separated from others or are only moderately overlapped. The remaining NOE volumes result from the manual division of extremely overlapped NOE peaks using the initial assumption that the structure was B-DNA like. The MORASS/rMD protocol was repeated many times with repeated adjustment of the overlapped volumes. This process slowly reduced the number of NOE violations and improved the structural statistics, without substantially changing the final structure, indicating that the inclusion of hundreds of poorly defined volumes was not necessary to determine the final structures. For the dithio containing sequences we could not assume a B-DNA conformation and fewer deconvoluted volumes from extremely overlapped NOE peaks were included in the calculations.

Structural comparison of CK14 and XBY6. The RMSD of the heavy atoms in the central 12 bp of the XBY6 and CK14 final structures is 2.2 Å. The XBY6 duplex is also 2.2 Å shorter in length than CK14. The dithioated internucleotide linkages to bases T10 and C11 are across the minor groove from another dithioated nt, C22, in the XBY6 duplex, and are near another dithioated nt, C24. Importantly, the widths of the phosphorus–phosphorus distances across the minor groove are considerably wider in XBY6 than in CK14 in this region (Fig. 8A, top two traces). The greatest change in the P–P distances across the minor groove occurs where two dithioated nts in XBY6, C11 and C22, are across the minor groove from each other. The distance from the C11 phosphorus atom to the C22 phosphorus atom is 13.70 Å in XBY6 but only 10.86 Å in CK14, a difference of 2.84 Å between the two structures. Likewise, one base step away, the minor groove width between the T10 phosphorus atom, which is dithioated in XBY6, and the T23 phosphorus atom is 14.10 Å in XBY6 but only 12.18 Å in CK14, a difference of 1.92 Å. One further base step removed, the minor groove distance between the phosphorus atoms of T9 and C24, which is di-

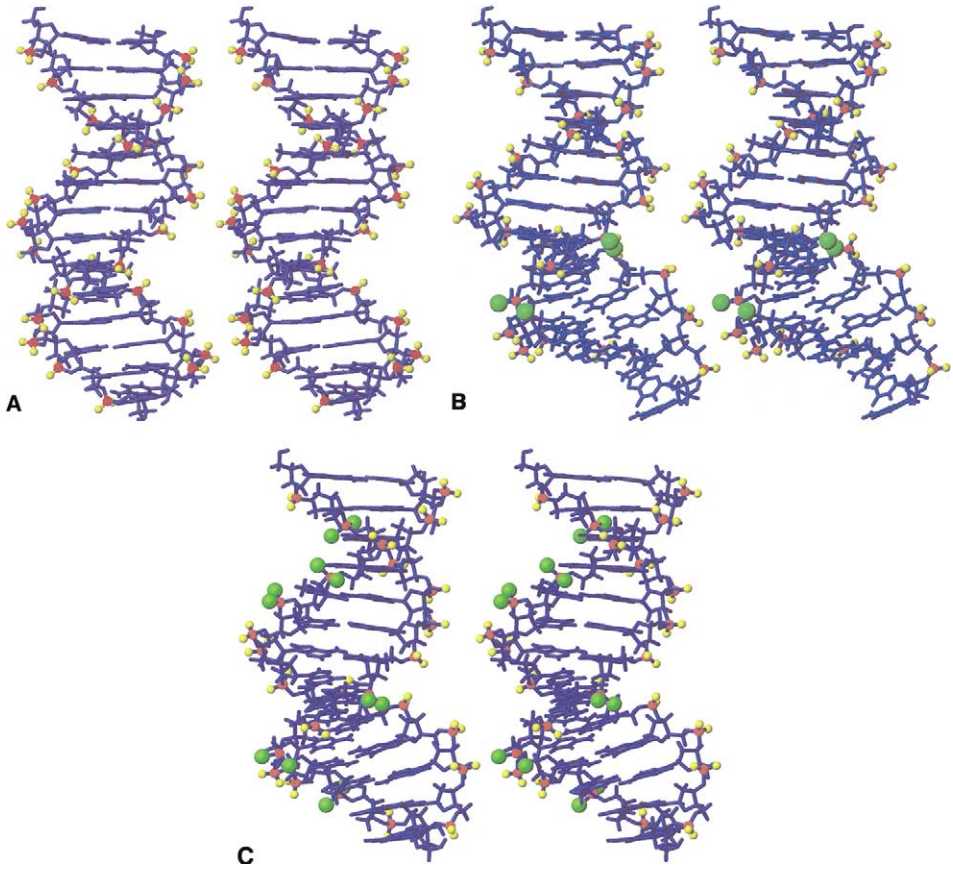

Fig. 7. The refined, averaged structures for CK14 (A), XBY2 (B), and XBY6 (C) shown in stereo-view. Phosphorus atoms are shown in red, nonbridging phosphoryl oxygens are shown in yellow, and sulfur atoms are shown in green.

thioated in XBY6, is 1.81 Å larger in XBY6 (13.35 Å) than it is in CK14 (11.54 Å). The effect of the dithioated nts is also observed on the other side of the C11–C22 minor groove. The distance between the phosphorus atoms of C12 and T21, neither of which are dithioated in XBY6 but which are next to two dithioated nts (C11 and C22) in XBY6, is 1.37 Å larger in XBY6 (12.84 Å) than it is in the CK14 duplex (11.47 Å). The remaining two dithioated substitutions in XBY6 at G17 and G27 are on the opposite side of the duplex helix from the previously discussed dithioated nts and are at opposing ends of the duplex. As a result of being isolated from other dithioated bases and their location near the duplex ends, these dithioate substitutions have little effect on the minor groove distance (see Table 3).

After conversion of the minor groove P–P distances by subtraction of the P–O or P–S bond lengths and the oxygen or sulfur van der Waals radii, the minor groove widths of XBY6 are still considerably larger than those of CK14 (Fig. 8A, bottom

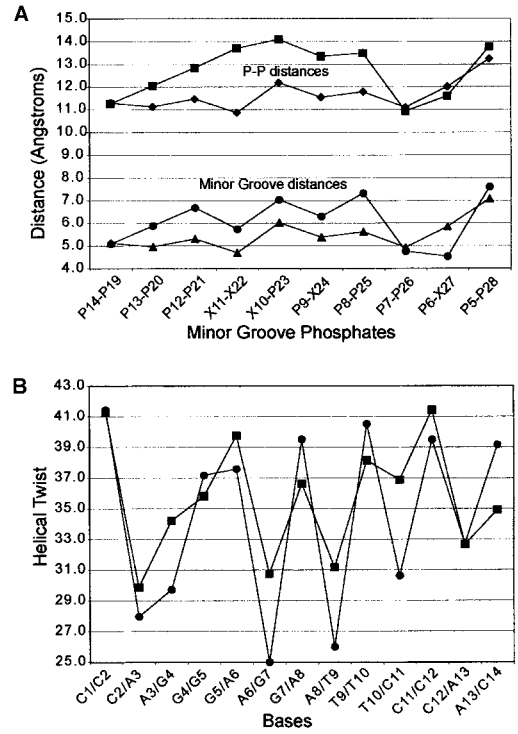

Fig. 8. (A) Comparison of P–P and minor groove distances across the minor grooves of CK14 (◆, ▲) and XBY6 (■, ●). (B) Helical twist of CK14 (■) and XBY6 (●) as a function of nucleotide position. Residue numbers are indicated as either a P or an X followed by the base number. P indicates a normal phosphate linkage in both duplexes while an X indicates that a dithioated phosphate linkage is present in the XBY6 duplex.

two traces). Interestingly, the pattern of minor groove variations seen in the normal CK14 oligonucleotide are largely reproduced in XBY6, indicating that minor groove distance variations due to the DNA sequence are not obliterated by the dithioation of specific phosphoryl groups.

Although the average helical twist of CK14 and XBY6, 35.7° and 34.4°, respectively, are very similar, an interesting pattern is observed in the helical twist parameter as a function of nucleotide (Fig. 8B). As in the case of the minor groove widths, similar patterns are observed for this parameter for both duplexes. However, near the center of the duplex where many of the dithioated bases are located, the pattern is exaggerated. For the helical twist parameters that are low in CK14, these parameters are 6–10° smaller in XBY6, while for the helical twist parameters that are larger in CK14, the twist is 2–3° larger. The larger differences between sequential helical twists may help relieve the strain associated with the widening of the minor groove.

Although the minor groove widths are greatly affected by the dithioate substitutions, the average major groove widths of CK14 and XBY6 (phosphate–phosphate

Table 3
Phosphate–phosphate distances and minor groove widths of CK14 and XBY6

Phosphates[b]	Minor groove phosphate–phosphate distances (Å)		Minor groove width (Å)[a]	
	CK14	XRY6	CK14	XBY6
P14–P19	11.28	11.25	5.12	5.09
P13–P20	11.12	12.04	4.96	5.88
P12–P21	11.47	12.84	5.31	6.68
X11–X22	10.86	13.70	4.70	5.74
X10–P23	12.18	14.10	6.02	7.04
P9–X24	11.54	13.35	5.38	6.29
P8–P25	11.78	13.49	5.62	7.33
P7–P26	11.09	10.92	4.93	4.76
P6–X27	12.00	11.59	5.84	4.53
P5–P28	13.24	13.77	7.08	7.61
	11.66 ± 0.70	12.71 ± 1.16	5.50 ± 0.70	6.10 ± 1.08

[a] Minor groove widths were determined by subtracting the bond lengths of P–O (1.48 Å) or P–S (1.98 Å) and the van der Waals radii of oxygen (1.60 Å) or sulphur (2.00 Å) from the phosphate–phosphate distances. The bond length values were taken from the structures and the van der Waals radii were taken from the AMBER force field parameters.

[b] Phosphates designated with P are normal phosphates in both CK14 and XBY6. Phosphates designated with X are normal phosphoryl groups in CK14 but are dithioated in XBY6.

distances), 17.3 ± 1.2 and 17.1 ± 1.6 Å, respectively, are very similar. However, because of the slightly greater average helical twist of the CK14 duplex relative to the XBY6 duplex, the major groove distances for the two duplexes are based on the distances of different phosphate groups. For example, in XBY6 the phosphorus atom of residue 6 (P6) is across the major groove from P18, while in CK14 P6 is across the major groove from P19.

In order to determine if the structural differences between CK14 and the thioated duplexes result from force field parameters rather than from differences in NMR-derived distance restraints, the structures of both CK14 and XBY6 were calculated from canonical B-DNA using 5 ps of rMD (using the appropriate distance restraints) with either the correct force field or the force field of the other duplex. The two structures determined for CK14 in this manner, with either the CK14 or XBY6 force fields, have an RMSD for the 12 central base pair (bp) heavy atoms (excluding nonbridging O or S atoms) of 0.85 Å. The same RMSD for the CK14 structure determined with the CK14 force field versus the CK14 ensemble average structure is 0.88 Å, while that determined with the XBY6 force field is 1.08 Å. Both of these values are within the range of the CK14 ensemble. The structures determined for XBY6 in this manner, using the XBY6 or CK14 force fields, had a similar 12 bp pairwise RMSD of 1.03 Å, and RMSDs versus the XBY6 ensemble average of 1.18 Å (XBY6 force field) and 1.19 Å (CK14 force field). Backbone atom overlays of these structures (Fig. 9) clearly show that the observed widening of the XBY6 minor

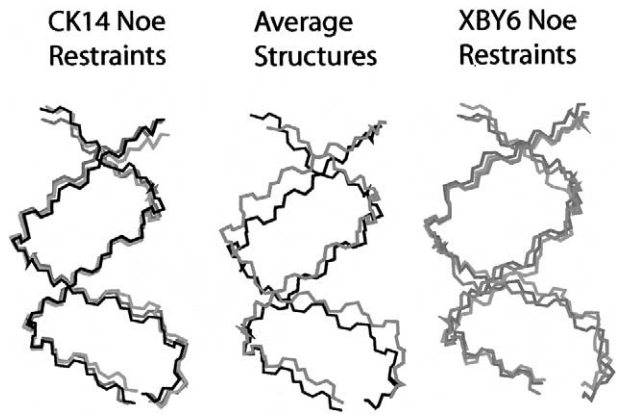

Fig. 9. Comparison of CK14 and XBY6 structures determined with both the CK14 and XBY6 force fields. The MORASS/MD average structures of CK14 (black) and XBY6 (grey) are shown in the central region. The CK14 (black) and XBY6 (grey) force fields were used to calculate both the CK14 (left) and the XBY6 (right) structures. Both the CK14 and XBY6 structures were adequately (determined using the improper force field, demonstrating that the structural differences observed are the result of NMR constraints rather than force field artifacts.

groove is reproducible using the XBY6 distance restraints and either the CK14 or XBY6 force fields.

4. Discussion

These results support prior structural work on the phosphorodithioate-modified duplexes, where significant distortions were previously observed in various duplex and stem loop structures [50,51]. Thus, the refined structure of the phosphorodithioate (pS_2) duplexes d($CGCT_PS_2TAAGCG)_2$, d(($CGCTpS_2TpS_2AAGCG)_2$, and d($CGCTpS_2TpS_2ApS_2ApS_2GCG)_2$ all show significant deviation from the unmodified phosphoryl parent duplex, including unwinding of the duplex. The minor groove width (P–P distance) of the 10-mer palindromic duplex with 8 dithioate substitutions is approximately 4 Å wider than that of the parent phosphoryl decamer d($CGCTTAAGCG)_2$ (4.2–9.4 Å). These distortions are similar to those we find for XBY-6. The opening of the minor groove and the unwinding of the [S_2]-ODN backbones indicate that the duplex has a more A-DNA-like conformation in the region surrounding the dithiophosphate modification.

Widening the minor groove increases the separation of the dithiophosphates across the two strands, presumably reducing electrostatic repulsion and explaining the duplex structural perturbations. However, as determined by our ab initio molecular orbital calculations [50,51,64], the charges on the sulfur atoms (−0.41 e) are considerably lower than those on the phosphoryl oxygens (−0.85 e). It is not correct, though, to consider the anionic repulsion alone in these perturbations, because the

net charge will be greatly reduced by the proximity and numbers of cations. Sulfur, being a much softer ion than oxygen, will not bind hard sodium ions as tightly as phosphoryl oxygens do. With fewer sodium ions in the solvation shell surrounding the dithiophosphates, the larger net repulsion between dithiophosphates may reflect their lower net charge neutralization. Our recent molecular dynamics simulation of a dithiophosphate duplex plus explicit Na^+ ions in water [50,64] support the lower affinity of sodium ions for the dithiophosphate. During the MD simulation, several of the sodium ions migrated away from the dithiophosphates, a behavior rarely observed when phosphoryl oxygens are present.

Role of metal ions in structural perturbations of DNA. As shown in Fig. 7, incorporation of dithioated groups leads to structural perturbations in the duplex [50], distorting the duplex into a more A-like conformation with sufficient dithioate substitutions. Monothiophosphates substituted in the DNA strand of DNA/RNA hybrids do not appear to dramatically alter duplex structures [52], although a recent structure by Nikonowicz and co-workers shows that monothioate substitutions can perturb stem-loop RNA structures [53].

We have argued that the origin of this thioate effect is the poorer coordination of the thio (and dithio) phosphates for metal ions. According to the recent electrostatic model proposed by Wilson et al. [54], minor groove width in normal backbone DNA is also dramatically influenced by the coordination of monovalent cations within the minor groove. The groove appears to widen as ions move away from the minor groove and narrow as they move closer consistent with the dithioate results.

In support of the important role of bound metal ions in defining the structure of duplexes, and in particular the minor groove width, we have recently completed the structures of several DNA duplexes with multiple substitutions of methylphosphonates for normal backbone phosphates in one of the strands (V. Thiviyanathan, et al., unpublished). The minor groove width (P–P separation) for both hetero duplexes was found to be generally wider (varying between 12.3–15.0 Å for the Rp isomer and 11.4–13.8 Å for the Sp isomer) compared to the minor groove in B-form phosphodiester DNA (11.5 Å). (Note: the Rp and Sp isomers only differ at a single phosphonate center, with all of the others being the same Rp stereochemistry.) Due to the presence of the bulky, neutral methyl groups in the phosphonate backbone, there would be diminished interactions between the Na^+ ions and the phosphate backbone resulting in the widening of the minor groove. Significantly, the minor groove width differs substantially between the Rp and Sp isomers, particularly at the phosphonate diastereomeric center at residue 13. The minor groove width (P–P separation) is widest (15.0 Å) for the Rp isomer but is *narrowest* for the Sp isomer (11.4 Å) at this position. While in the Rp isomer the methyl group is oriented towards the solvent, it is also pointed toward the minor groove. For the Sp isomer the phosphoryl group is oriented towards the minor groove. One explanation for these differences could simply be the greater steric bulk of the methyl group oriented towards the solvent/minor groove in the Rp isomer. Alternatively, if sodium or other cations are indeed bound in the minor groove, as supported by recent X-ray studies of normal backbone duplex oligonucleotides [54], then only in the case of the Sp isomer could the phosphoryl group of the phosphonate help coordinate a metal ion across the minor groove to a phosphate on the opposing strand.

Thus, as in the case of the neutral methyl phosphonates, the minor grooves are considerably expanded in dithioated DNA duplexes, especially when two dithioates are opposed across the minor groove. Dithioates coordinate metal ions such as sodium ions much poorer than phosphates and this increase in minor groove width (P–P separation increasing from 11.5 to 14 Å) is such as to convert a normal B-form duplex to a duplex that has more A-DNA-like character.

Origin of enhanced protein affinity for dithioate aptamers. As noted above, sulfurization of the phosphoryl oxygens of oligonucleotides often leads to their enhanced binding to numerous proteins. The dithioate agents, for instance, appear to inhibit viral polymerases at much lower concentrations than do the monothiophosphates, which in turn are better than the normal phosphates with K_d in the sub-nM range for HIV-1 RT [55]. For HIV-1 RT, dithioates bind 28–600 times more tightly than the normal aptamer oligonucleotide or the monothio analogue.

Oligonucleotides possessing high monothio- or dithiophosphate backbone substitutions thus appear to be "stickier" toward proteins than normal phosphate esters, an effect often attributed to "nonspecific interactions". Based upon our earlier NMR structural studies of dithiophosphate-substituted oligonucleotides, we have suggested that one explanation for the higher affinity of the thiosubstituted DNAs is the relatively poor cation coordination of the polyanionic backbone [50]—sulfur being a soft anion does not coordinate as well to hard cations like Na^+, unlike the hard phosphate oxyanion. The thiosubstituted phosphate esters then act as "bare" anions, and since energy is not required to strip the cations from the backbone upon binding, these agents can in principle bind even tighter to proteins.

Even in specific protein-nucleic acid contacts, sulfurization of the internucleotide linkages can lead to enhanced binding [55,56] (or to reduced affinity). This can be quite important since most of the direct contacts between DNA binding proteins and their binding sites are to the phosphate groups [57,58], as is true for NF-κB [45–48]. We can take advantage of this "stickiness" to enhance the specificity and affinity of thio- and dithiophosphate agents for a protein target. However, we need to optimize the total number of thioated phosphates to decrease nonspecific binding to nontarget proteins and enhance only the specific favorable interactions with the target protein.

Is the enhanced nonspecific protein binding of the di- and monothiophosphate agents (relative to the unmodified phosphoryl backbone) attributable to the loosened coordination shell of cations surrounding the oligonucleotide? Binding of the agents to a nucleic acid-binding protein such as NF-κB requires stripping many of the cations from the agent. Is this then easier for the sulfur-modified phosphoryl agents? It has been suggested that this is due to increased hydrophobicity of the sulfur-containing ODNs [55]. However, our structural analysis suggests that it is at least partially an electrostatic effect. Quite possibly, the [S_2]-ODN could operate via different inhibitory mechanisms, depending upon the structural perturbations created by the number and position of the sulfur modifications. It will ultimately be important to establish the origin of these specific and "nonspecific" mechanisms [59,60].

We hypothesize that one of the reasons for the enhanced binding of the thioated aptamers to the proteins is that it is easier to dissociate the bound cations to the thioated aptamers than to the unmodified aptamers. Our model of the XBY-6·NF-

κB complex strongly supports this hypothesis with the dithiophosphates in close proximity to basic side chains. However, a secondary effect of the dithioation is to perturb the structure to a more A-like conformation. Thus the enhanced binding of XBY-6 could be due to a better shape-selectivity of the thioated aptamer as well.

Acknowledgments

We acknowledge the helpful comments and support by Robert Shope and Judy Aronson. We acknowledge the seminal development of the molecular mechanics method by Frank Westheimer [61,62], which has provided the intellectual framework for other force field methods, including the restrained molecular dynamics used in our current calculations of NMR solution structures. David Gorenstein wishes to express his appreciation to Frank Westheimer for teaching him that even simple, back of the envelope calculations can be very instructive and that rigor and excellence in science is paramount. To Frank, on his 90th birthday.

References

[1] I.M. Verma, J.K. Stevenson, E.M. Schwarz, D. Van Antwerp, S. Miyamoto, Genes Dev. 9 (1995) 2723–2735.
[2] U. Siebenlist, G. Franzoso, K. Brown, Annu. Rev. Cell Biol. 10 (1994) 405–455.
[3] P.A. Baeuerle, Curr. Biol. 8 (1998) R19–R22.
[4] P.J. Barnes, M. Karin, New Engl. J. Med. 336 (1997) 1066–1071.
[5] P.A. Baeuerle, V.R. Baichwal, Adv. Immunol. 65 (1997) 111–137.
[6] E. Caldenhoven, J. Liden, S. Wissink, A. Van de Stolpe, J. Raaijmakers, I. Koenderman, S. Okret, J. Gustafsson, P.T. Van der Saag, Mol. Endocrinol. 9 (1995) 401–412.
[7] C.K. Sen, L. Packer, FASEB J. 10 (1996) 709–720.
[8] H.L. Pahl, B. Kraub, K. Schulze-Osthoff, E.B.M. Traenekner, T. Parks, C. Meyers, P. Waring, A. Muehlebacher, P.A. Czernilofsky, P.A. Baeuerle, J. Exp. Med. 183 (1996) 1829–1840.
[9] A. Beg, W.C. Sha, R.T. Bronson, S. Ghosh, D. Baltimore, Nature 376 (1995) 167–169.
[10] F. Köntgen, R.J. Grumont, A. Strasser, D. Metcalf, R. Li, D. Tarlinton, S. Gerondakis, Genes Dev. 9 (1995) 1965–1977.
[11] W.C. Sha, H.C. Liou, E.I. Tuomanen, D. Baltimore, Cell 80 (1995) 321–330.
[12] I. Kitajima, T. Shinohara, J. Bilakovics, D.A. Brown, X. Xu, M. Nerenberg, Science 258 (1992) 1792–1795.
[13] A. Calogero, G.A.P. Hospers, N.H. Mulder, Pharm. World Sci. 19 (1997) 264–268.
[14] A. Bielinska, R.A. Shivdasani, L.Q. Zhang, G.J. Nabel, Science 250 (1990) 997–1000.
[15] H.W. Sharma, J.R. Perez, K. Higgins-Sochaski, R. Hsiao, R. Narayanan, Anticancer Res. 16 (1996) 61–69.
[16] A.R. Khaled, E.J. Butfiloski, E.S. Sobel, J. Schiffenbauer, Clin. Immnol. Immunopathol. 86 (1998) 170–179.
[17] Y. Sawa, R. Morishita, K. Suzuki, K. Kagisaki, Y. Kaneda, K. Maeda, K. Kadoba, H. Matsuda, Circulation 96 (1997) II-280–II-284.
[18] J.F. Schmedtje, W.L. Ji, R.N. Dubois, M.S. Runge, J. Biol. Chem. 272 (1997) 601–608.

[19] M.F. Romano, A. Lamberti, P. Tassone, F. Alfinito, S. Constanti, F. Chiurazzi, T. Defrance, P. Bonelli, F. Tuccillo, M.C. Turco, S. Venuta, Blood 92 (1998) 990–995.
[20] Y.G. Park, M. Nesterova, S. Agrawal, Y.S. Cho-Chung, J. Biol. Chem. 274 (1999) 1573–1580.
[21] R. Morishita, G.H. Gibbons, M. Horiuchi, K.E. Ellison, M. Nakama, L. Zhang, Y. Kaneda, T. Ogihara, V.J. Dzau, Proc. Natl. Acad. Sci. USA 92 (1995) 5855–5859.
[22] G. Jin, P.H. Howe, J. Biol. Chem. 272 (1997) 26620–26626.
[23] R. Morishita, J. Higaki, N. Tomita, T. Ogihara, Circ. Res. 82 (1998) 1023–1028.
[24] Y.S. Cho-Chung, Antisense Nucleic Acid Drug Dev. 8 (1998) 167–170.
[25] Tomita N, R. Morishita, J. Higaki, T. Ogihara, Exp. Nephrol. 5 (1997) 429–434.
[26] M.J. Mann, Antisense Nucleic Acid Drug Dev. 8 (1998) 171–176.
[27] C. Boccaccio, M. Ando, L. Tamagnone, A. Bardelli, P. Michieli, C. Battistini, P.M. Comoglio, Nature 391 (1998) 285–288.
[28] S.D. Putney, S.J. Benkovic, P.R. Schimmel, Proc. Natl. Acad. Sci. USA 78 (1981) 7350–7354.
[29] W.T. Wiesler, M.H. Caruthers, J. Org. Chem. 61 (1996) 4272.
[30] X. Yang, S. Fennewald, B.A. Luxon, J. Aronson, N.K. Herzog, D.G. Gorenstein, Bioorg. Med. Chem. Lett. 9 (1999) 3357–3362.
[31] Q. Xu, K. Musier-Forsyth, R.P. Hammer, G. Barany, Nucleic Acids Res. 24 (1996) 1602–1607.
[32] S.H. Smallcombe, S.L. Patt, P.A. Keifer, J. Magn. Reson. 117 (1995) 295–303.
[33] Y.S. Cho-Chung, Antisense Nucleic Acid Drug Dev. 8 (1998) 167–170.
[34] U. Piantini, O.W. Sorenson, R.R. Ernst, J. Am. Chem. Soc. 104 (1982) 6800–6801.
[35] E.J. Schurter, H.J.C. Yeh, J. Sayer, M. Lakshman, K, H. Yagi, D.M. Jerina, D.G. Gorenstein, Biochemistry 34 (1995) 1364–1375.
[36] R. Meadows, C.B. Post, B.A. Luxon, D.G. Gorenstein, MORASS Program, University of Texas Medical Branch, Galveston, TX, 1996.
[37] AMBER 5. D.A. Case, D.A. Pearlman, J.W. Caldwell, T.E.I. Cheatham, W.S. Ross, C.L. Simmerling, T.A. Darden, K.M. Merz, R.V. Stanton, A.L. Cheng, J.J. Vincent, M. Crowley, D.M. Ferguson, R.J. Radmer, G.L. Seibel, U.C. Singh, P.K. Weiner, P.A. Kollman, AMBER 5, University of California, San Francisco, 1997.
[38] W.S. Ross, CARNAL, University of California, San Francisco, CA, 1994.
[39] C.I. Bayly, T. Cieplak, W.D. Cornell, P.A. Kollman, J. Chem. Phys. 97 (1993) 10269–10280.
[40] C.B. Post, R. Meadows, D.G. Gorenstein, J. Am. Chem. Soc. 112 (1990) 6796.
[41] B.A. Borgias, T.L. James, J. Magn. Res. 87 (1990) 475–487.
[42] R. Koradi, M. Billeter, K. Wuthrich, MOLMOL: A Program for Display and Analysis of Macromolecular Structure, Institute for Molecular Biology and Biophysics, Swiss Federal Institute of Technology, Zürich, Switzerland, 1996.
[43] C.E.A.F. Schafmeister, W.S. Ross, V. Romanovski, LEaP, University of California, San Francisco, CA, 1995.
[44] T.E. Ferrin, C.C. Huang, L.C. Jarvis, R. Langridge, J. Mol. Graphics 6 (1988) 13–27.
[45] F.E. Chen, D.B. Huang, Y.Q. Chen, G. Ghosh, Nature 5 (1998) 391–410.
[46] C.W. Müller, F.A. Rey, M. Sodeoka, G.L. Verdine, S.C. Harrison, Nature 373 (1995) 311–317.
[47] Y.Q. Chen, S. Ghosh, G. Ghosh, Nat. Struct. Biol. 5 (1998) 67.
[48] G. Ghosh, G. van Duyne, S. Ghosh, P.B. Sigler, Nature 373 (1995) 303–310.
[49] K. Wuthrich, NMR of Proteins and Nucleic Acids, Wiley, New York, 1986.
[50] Y.S. Cho, F.C. Zhu, B.A. Luxon, D.G. Gorenstein, J. Biomol. Struct. Dynam. 11 (1993) 685–702.

[51] D.G. Gorenstein, C. Karslake, J.N. Granger, Y. Cho, M.E. Piotto, in: E.N. Walsh, E.J. Griffith, R.W. Parry, C.D. Quin (Eds.), Phosphorus Chemistry (ACS Symposium Series), American Chemical Society, Washington, DC, 1992, pp. 202–217.
[52] C. Gonzalez, W. Stec, M.A. Reynolds, T.L. James, Biochemistry 34 (1995) 4969–4982.
[53] J.S. Smith, E.P. Nikonowicz, Biochemistry 39 (2000) 5642–5652.
[54] D. Hamelberg, L. McFail-Isom, L.D. Williams, W.D. Wilson, J. Am. Chem. Soc. 122 (2000) 10513–10520.
[55] W.S. Marshall, M.H. Caruthers, Science 259 (1993) 1564–1570.
[56] J.F. Milligan, O.C. Uhlenbeck, Biochemistry 28 (1989) 2849–2855.
[57] Z. Otwinowski, R.W. Schevitz, R.G. Zhang, C.L. Lawson, A. Joachimiak, R.Q. Marmorstein, B.F. Luisi, P.B. Sigler, Nature 335 (1988) 321.
[58] D.G. Gorenstein, Chem. Rev. 94 (1994) 1315–1338.
[59] G. Zon, M. Matsukura, Int. J. Immunother. 4 (1990) 187–191.
[60] C.A. Stein, Leukemia 6 (1992) 967–974.
[61] F.H. Westheimer, J.E. Mayer, J. Chem. Phys. 14 (1946) 733.
[62] F.H. Westheimer, J. Chem. Phys. 15 (1947) 252.
[63] D.J. King, S.E. Bassett, X. Li, S.A. Fennewald, N.K. Herzog, B.A. Luxon, R. Shope, D.G. Gorenstein, Biochemistry 41 (2002) 9696–9706.
[64] D.E. Volk, T.D. Power, D.G. Gorenstein, B.A. Luxon, Tetr. Lett. 43 (2002) 4443–4447.